Alternative low-cost approach to the synthesis of magnetic iron oxide nanoparticles by thermal decomposition of organic precursors

2013 Nanotechnology 24 175601

(http://iopscience.iop.org/0957-4484/24/17/175601)

Nanotechnology **24** (2013) 175601 (11pp) doi:10.1088/0957-4484/24/17/175601

Alternative low-cost approach to the synthesis of magnetic iron oxide nanoparticles by thermal decomposition of organic precursors

I O Perez De Berti[1], M V Cagnoli[1], G Pecchi[2], J L Alessandrini[3,4], S J Stewart[3], J F Bengoa[1,4] and S G Marchetti[1]

[1] CINDECA, CONICET—Universidad Nacional de La Plata, Facultad de Ciencias Exactas, Calle 47 N° 257, 1900, La Plata, Argentina
[2] Departamento de Físico Química, Facultad de Ciencias Químicas, Universidad de Concepción, Casilla 160-C Concepción, Chile
[3] IFLP-CCT-La Plata-CONICET and Departamento de Física, Facultad de Ciencias Exactas, C. C. 67, Universidad Nacional de La Plata, 1900 La Plata, Argentina
[4] Comisión de Investigaciones Científicas de la Provincia de Buenos Aires (CIC), La Plata, Argentina

E-mail: march@quimica.unlp.edu.ar

Received 14 January 2013, in final form 5 March 2013
Published 2 April 2013
Online at stacks.iop.org/Nano/24/175601

Abstract
A new approach to thermal decomposition of organic iron precursors is reported, which results in a simpler and more economical method to produce well crystallized γ-Fe_2O_3 nanoparticles (NPs) with average sizes within the 3–17 nm range. The NPs were characterized by TEM, SAED, XRD, DLS-QELS, Mössbauer spectroscopy at different temperatures, FT-IR and magnetic measurements. The obtained γ-Fe_2O_3 NPs are coated with oleic acid and, in a lower quantity, with oleylamine (about 1.5 nm in thickness). It was shown that changing operative variables allows us to tune the average particle diameters and obtain a very narrow or monodisperse distribution of sizes. The γ-Fe_2O_3 NPs behave superparamagnetically at room temperature and their magnetization saturation is reduced by about 34% in comparison with bulk maghemite. The results indicate that the distance between two neighbour NPs, generated by the coating, of about 3 nm is insufficient to inhibit interparticle magnetic interactions when the average diameter is 8.8 nm. The good quality of the NPs, obtained through the present low-cost and easy-handling process, open a new perspective for future technological applications.

S Online supplementary data available from stacks.iop.org/Nano/24/175601/mmedia

(Some figures may appear in colour only in the online journal)

1. Introduction

Superparamagnetic iron oxide nanoparticles (SPIONs) have attracted a great deal of attention due to their chemical and physical properties, which differ significantly from those of bulk material, and their potential applications. Between actual and potential applications the following can be mentioned: in biomedical areas, *in vivo* drug delivery [1, 2], *in vitro* cell separation [3], immunoassay [4], contrast agents in magnetic resonance imaging [5–7], and hyperthermia [8]; in technological areas, magnetic storage [9, 10], magnetic ink printing [11], magnetic refrigeration systems [12], and catalysis [13].

Most of these applications require well dispersed chemically stable nanoparticles (NPs) having uniform size and shape, superparamagnetic behaviour, and high

saturation magnetization values (M_s). Furthermore, the preparation method would be reproducible without any complex purification procedure, such as ultracentrifugation, size-exclusion chromatography, etc.

Different methodologies to obtain SPIONs have been reported in the literature. The classical synthetic techniques of iron oxide NPs have relied on the coprecipitation of Fe^{2+} and Fe^{3+} ions by a base. The main advantage of the coprecipitation process is that a large number of NPs can be synthesized. However, the pH of the reaction mixture, the temperature, the ionic strength of the media, and the ageing time have to be adjusted in a careful way, and the process towards production of monodisperse NPs smaller than 20 nm has a only very limited success [10].

Water-in-oil microemulsions are currently being used to synthesize SPIONs with a narrow size range and uniform physical properties [14]. This system is formed by well defined nanodroplets of the aqueous phase, dispersed by the assembly of surfactant molecules in a continuous hydrocarbon phase. Therefore, the size of the NPs can be controlled by regulating the size of the aqueous droplet core. Significant disadvantages of the microemulsion methods are the difficulty of their scale-up, and the adverse effects of residual surfactants on the particle properties [15].

Aerosol technologies, such as spray and laser pyrolysis, are attractive because they are continuous chemical processes that allow high rate production [16]. However, the NPs obtained by these technologies may be poorly crystalline and the size uniformity is hard to control [17].

Alternative methods based on the thermal decomposition of organic iron precursors have been demonstrated to be very successful in the preparation of iron oxide NPs with controllable size and high quality. Thus, Rockenberger *et al* [18] reported the preparation of monodispersed maghemite by decomposition of iron cupferronates (Cup: $C_6H_5N(NO)O^-$) in the presence of octylamine and trioctylamine. Since then, Hyeon *et al* [19] have prepared monodisperse γ-Fe_2O_3 NPs in the size range of 4–16 nm by decomposing $Fe(CO)_5$ complexes in octyl ether at 573 K in the presence of oleic acid as a capping agent. The narrowness of the NP distribution produces superlattice formation. However, $Fe(CO)_5$ is highly toxic, air sensitive, and very expensive. On the other hand, Sun and co-workers [20] have synthesized Fe_3O_4 by heating $Fe(acac)_3$ with oleylamine, oleic acid, and 1,2-hexadecanediol. In comparison to other acetylacetonates or acetate precursors, $Fe(acac)_3$ is less costly and has low moisture sensitivity. Furthermore, the NPs are of comparable uniformity with other recipes and monodispersed.

Unfortunately, in most of the reported syntheses, only small quantities of monodisperse nanocrystals can be produced and, in addition, some of the reagents used are very expensive. Therefore, the development of new synthesis methods, more economical and simpler, is necessary, in order to produce future technological applications. With this aim, we have analysed the market prices of the reagents used in Sun's recipe [20], and we found that the reducing agent (1,2-hexadecanediol) represents about of 86% of the total cost. Furthermore, the inert atmosphere requirement (N_2) produces a drawback if larger product quantities need to be produced. In order to reduce the cost and simplify the handling process, in the present work, we present a new approach to the synthesis by thermal decomposition, by removing the reducing agent and the inert atmosphere. In this situation γ-Fe_2O_3 would be produced instead of Fe_3O_4. Therefore, we must check that the obtained NPs are monodisperse and crystalline and that the magnetization saturation is of the same order as that obtained by Sun *et al* [20].

2. Experimental section

The syntheses were carried out using commercially available reagents. Diphenyl ether (99%), oleic acid (90%), oleylamine (>70%) and iron(III) acetylacetonate (97%) were purchased from Aldrich Chemical Co and dibenzyl ether (98%) from Fluka. These reactants, ethanol, and hexane, were used as they were received.

2.1. Synthesis of iron oxide NPs

In the first synthesis the same reagent quantities as used by Sun *et al* [20] to produce 4 nm Fe_3O_4 NPs were utilized, but without the reducing agent (1,2-hexadecanediol) and the N_2 flow. Thus, $Fe(acac)_3$ (4 mmol), oleic acid (12 mmol), oleylamine (12 mmol), and diphenyl ether (20 ml, boiling point: 532 K) were mixed and magnetically stirred under air (iron salt:surfactant:solvent molar ratio = 1:6:158). The mixture was heated to 473 K for 45 min and then heated to reflux (538 K) for another 45 min. The black–brown mixture was cooled to room temperature by removing the heat source. Under ambient conditions, ethanol (80 ml) was added to the mixture, and a black material was precipitated and separated via centrifugation. The black product was dispersed in hexane in the presence of oleic acid (0.1 ml) and oleylamine (0.1 ml). Centrifugation (6000 rpm, 10 min) was applied to remove any un-dispersed residue. The product, named M1, was then precipitated with ethanol, centrifuged (6000 rpm, 10 min) to remove the solvent, and re-dispersed into hexane.

In order to study the effect of some operative variables, other syntheses were carried out changing the iron salt:surfactant:solvent molar ratio. The following ratios were used: 1:3:158, 1:30:158 and 1:30:316. The products thus obtained were called M2, M3 and M4 respectively. Another reaction was done in the same way as for M1 except that the solvent diphenyl ether was changed to benzyl ether (boiling point: 568–571 K). This sample was called M5. All samples were purified in the same way as M1.

2.2. Characterization of iron oxide NPs

The samples were characterized by transmission electron microscopy (TEM), selected-area electron diffraction (SAED), x-ray diffraction (XRD), dynamic light scattering/quasielastic light scattering (DLS-QELS), Mössbauer spectroscopy (MS) between 298 and 13 K, magnetic measurements and Fourier transform infrared spectroscopy (FT-IR).

Samples for TEM analysis were prepared by drying a dispersion of the particles on amorphous carbon coated copper grids. TEM micrographs were obtained on a JEOL model JEM-1200 EX II microscope. The structure and the crystallinity of the particles were characterized using electron diffraction.

XRD patterns were measured using a standard Philips PW 1710 automated powder x-ray diffraction system with diffracted-beam graphite monochromator using Cu Kα radiation ($\lambda = 1.5406$ Å) in the range $2\theta = 25°$–$85°$ with steps of 0.02° and counting time of 16 s/step.

In the DLS-QELS measurements, the time correlation function $G(q, t)$ of the light scattering intensity was measured at the scattering angle $\theta = 90°$ with a goniometer ALV/CGS-5022F with multiple tau digital correlator ALV-5000/EPP covering a 10^{-6}–10^{3} s time range. The light source was a helium/neon laser ($\lambda = 632.8$ nm) operating at 22 mW. All of the measurements were carried out at room temperature (details appear in the supplementary file available at stacks.iop.org/Nano/24/175601/mmedia). In order to obtain appropriate estimations of the size of the particles, number and weight average hydrodynamic radii were calculated from the time correlation function with the package CONTIN [21].

Mössbauer spectra were obtained in transmission geometry with a 512-channel constant acceleration spectrometer. A source of ^{57}Co in a Rh matrix of nominally 50 mCi was used. Velocity calibration was performed against a 12 μm thick α-Fe foil. All isomer shifts (δ) mentioned in this paper are referred to this standard. The temperature was varied between 13 and 298 K using an ARS closed cycle cryocooler model ARS 8200. The spectra were evaluated using the Recoil spectral analysis software [22]. Although some spectra display magnetic relaxation, for simplicity Lorentzian lines with equal widths were considered for each component. The spectra were folded to minimize geometric effects.

The magnetic measurements were carried out using a multipurpose physical magnetic system (MPMS) superconducting quantum interference device (SQUID) from Quantum Design. The magnetization versus magnetic field (M–H) curves were recorded at 6 and 300 K up to a maximum magnetic field of 50 kOe. Thermal dependences of M under zero field cooling (ZFC) and field cooling (FC) conditions were recorded using a field H_{FC} of 100 Oe. After these measurements, each sample was calcined in air to suppress the organic matter. Then, the iron oxide was dissolved with HCl and the iron concentration was determined by a colorimetric method [23]. In this way, all magnetic results can be normalized by the real mass of the NPs, and the saturation magnetizations are free of a misinterpretation produced, for example, by the mass of the surfactant adsorbed on the NPs surface.

Infrared spectra of dried particles and pure oleic acid and oleylamine mixed with KBr (1:100) were obtained on a Jasco FT/IR-4200 spectrometer equipped with a PIKE diffuse IR cell with a resolution of 1 cm^{-1}. Two hundred to four hundred scans were accumulated in each case.

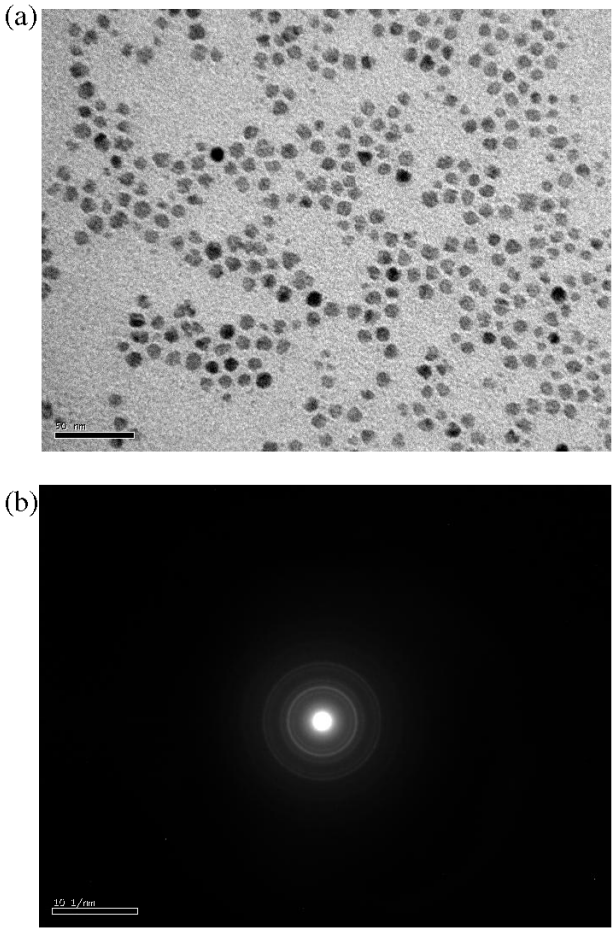

Figure 1. (a) TEM image of M1 sample. (b) Electron diffraction image of M1 sample.

3. Results and discussion

3.1. Phase identification and particle sizes distribution

TEM analysis shows that M1 and M2 samples have a very narrow size distribution. Figures 1(a) and 2(a) display typical TEM images from representative NPs of both preparations deposited from their hexane dispersions and dried under ambient conditions. We observed that the particles have nearly spherical shape. Furthermore, a slight faceting may be found in some particles, especially in M2. Figure 3 displays the histograms obtained considering 636 and 1165 particles for M1 and M2, respectively. Both histograms were fitted using a log-normal distribution, in agreement with previous studies showing that particles too small to display crystal habit (i.e. lower than 20 nm) present a log-normal size distribution [24]. The statistical parameters are displayed in table 1. It can be seen that the average size of M1 is about twice that obtained by Sun and colleagues for his Fe_3O_4 NPs [20] (4 nm versus 8.8 nm). We associate this result with the absence of the reducing agent (1,2-hexadecanediol) in our synthesis. Furthermore, in M2 there is an increase of the average diameter and a widening of the distribution with respect to M1. This latter effect could be attributed to the decrease of the surfactant content in the reaction mixture.

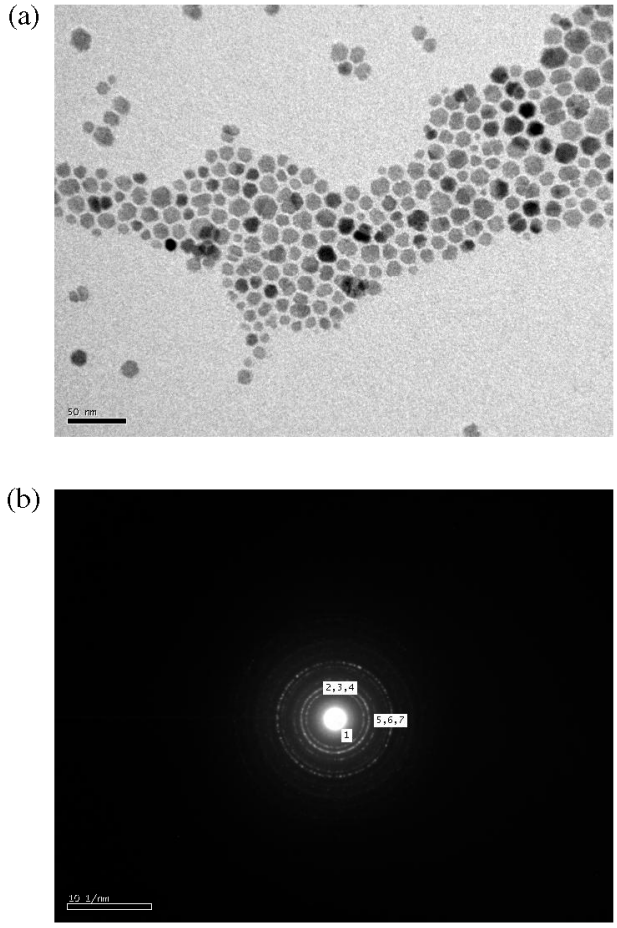

Figure 2. (a) TEM image of M2 sample. (b) Electron diffraction image of M2 sample.

Table 1. Statistical parameters of M1 and M2 samples obtained from TEM measurements. μ_g, geometric mean; σ_g, standard geometric deviation; μ_a, arithmetic mean; $P(\mu_g - \sigma_g \leq x \leq \mu_g + \sigma_g)$ (%), population percentage in the range $\pm\sigma_g$.

Samples	μ_g	σ_g	μ_a	Mode	$P(\mu_g - \sigma_g \leq x \leq \mu_g + \sigma_g)(\%)$
M1	8.8	1.2	8.9	8.5	55
M2	11.3	1.2	11.5	10.9	44

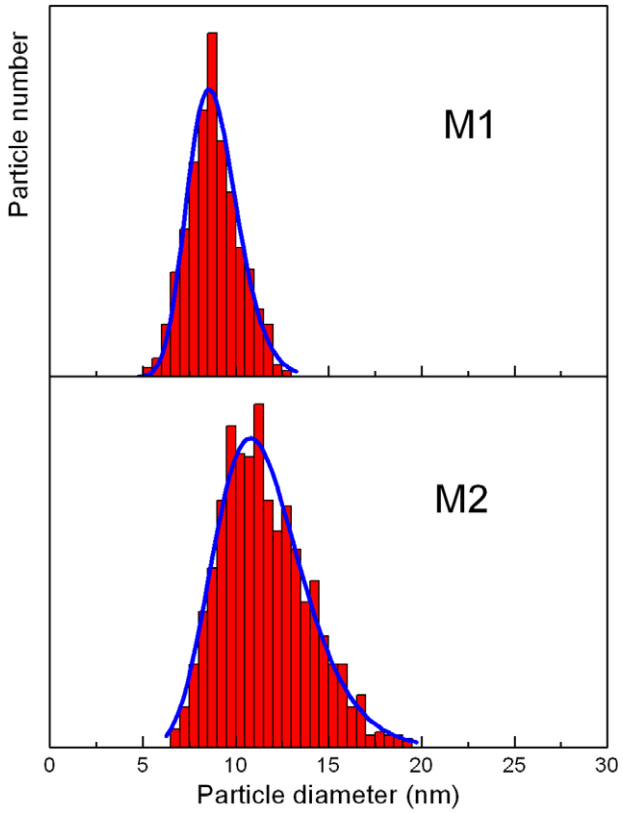

Figure 3. Size distributions of samples M1 and M2 from TEM measurements. Solid (blue) lines were obtained fitting the results by assuming a log-normal distribution.

To get structural information, the electron diffraction of a selected area (SAED) was acquired and analysed. Table 2 shows the measured lattice spacing based on the rings in the diffraction pattern (figures 1(b) and 2(b)) and compares them to the known lattice spacing for bulk γ-Fe_2O_3 and Fe_3O_4 along with their respective (*hkl*) indices from the PDF database (the presence of α-Fe_2O_3 can be discarded, since its typical reflections are absent). The absence of α-Fe_2O_3 was verified by XRD, as can be seen in figure 4. This diffractogram only displays peaks characteristic of spinel structure. Taking into account that γ-Fe_2O_3 and Fe_3O_4 have nearly identical diffraction patterns (they have almost the same spinel structure with only $\approx$1% difference between their lattice constants [25]), it is not possible to distinguish γ-Fe_2O_3 from Fe_3O_4 either by SAED or by XRD. As will be shown below, we use Mössbauer spectroscopy in order to achieve this aim. The diffraction rings of the M1 sample are more diffuse than those produced by M2 ((1 1 1) and (4 2 2) planes cannot be detected). This result could be linked with the lower particle size of the M1 sample.

In order to check the size distribution values obtained by TEM, we have also performed DLS-QELS experiments. It worth mentioning that DLS-QELS measurements are easier and faster to carry out and, in addition, provide more statistically significant information than TEM. Comparing the results from the two techniques (tables 1 and 3), we observe that there is an excellent concordance between the statistical values of M1. However, for M2, this agreement gets worse, probably due to the broadening of the size distribution of this sample. Therefore, the average size values and the distributions obtained from DLS-QELS are reliable, especially if the size distributions are narrow. Taking into account all these advantages, we used this technique to estimate sizes and distributions in all samples (figure 5). The effect of the different synthesis conditions is evident. Indeed, a decreasing of the surfactant quantity, with respect to the ratio used to synthesize M1, produces particles of about double the size, but with a broadened size distribution. The population percentage in the range $\pm\sigma_g$ (geometric standard deviation) decreases from 81% to 37%. Instead, if the surfactant quantity is increased fivefold with respect to M1

Table 2. Measurements of the lattice spacing, d (nm), for M1 and M2, based on the electron diffraction rings in figures 1 and 2 and standard spacing for γ-Fe_2O_3 and Fe_3O_4 along with their respective (*hkl*) indices from the PDF database.

(*hkl*)	M1 (nm)	M2 (nm)	Standard γ-Fe_2O_3 PDF 895892 (nm)	Standard Fe_3O_4 PDF 893854 (nm)
(1 1 1)	n.d.[a]	0.4709	0.482	0.4852
(2 2 0)	0.2991	0.2985	0.2953	0.2967
(3 1 1)	0.2556	0.2527	0.2518	0.2532
(4 0 0)	0.2114	0.2092	0.2089	0.2099
(4 2 2)	n.d[a]	0.1706	0.1703	0.1715
(5 1 1)	0.1609	0.1616	0.1607	0.1616
(4 4 0)	0.1490	0.1474	0.1476	0.1485

[a] n.d.: not detected.

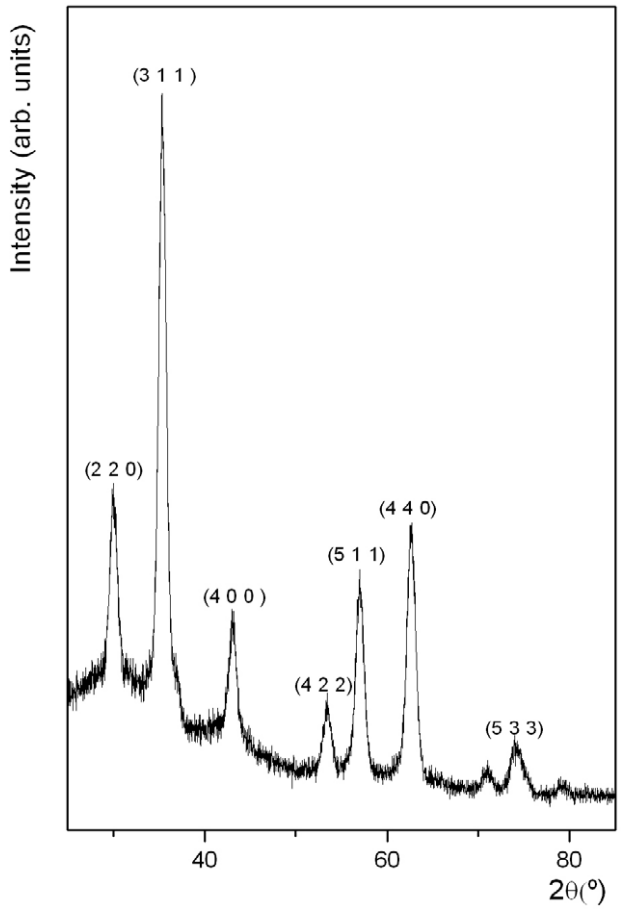

Figure 4. DRX of M1 sample. Miller indices (*hkl*) of main lines are indicated.

(sample M3), the average size decreases about threefold, but more importantly the distribution becomes monodispersed: 99% of the population is included in the range $\pm\sigma_g$. When the surfactant quantity remains constant and the solvent is increased twofold (sample M4), no changes, in either the average size or the distribution width, are detected. Finally, if the solvent diphenyl ether is replaced by benzyl ether (higher boiling point: 568–571 K), an average size similar to that of M2 is obtained (sample M5), but the distribution width of this sample is markedly lower than that of M2.

From the analysis of TEM, SAED, XRD and DLS-QELS results we conclude that this synthesis method provides well

Table 3. Statistical parameters of M1, M2, M3, M4 and M5 samples obtained from DLS measurements. μ_g, geometric mean; σ_g, standard geometric deviation; μ_a, arithmetic mean; $P(\mu_g - \sigma_g \leq x \leq \mu_g + \sigma_g)$ (%), population percentage in the range $\pm\sigma_g$.

Samples	μ_g	σ_g	μ_a	Mode	$P(\mu_g - \sigma_g \leq x \leq \mu_g + \sigma_g)(\%)$
M1	9.5	1.2	9.6	9.2	81
M2	17.0	1.1	17.1	16.8	37
M3	3.9	1.1	3.9	3.9	99
M4	3.5	1.2	3.6	3.4	94
M5	16.3	1.1	16.4	16.2	52

crystallized and monodispersed iron oxide NPs of average sizes between 3 and 17 nm. To get these results it is necessary to carefully manipulate the iron salt: surfactant:solvent molar ratio or the nature of the solvent.

3.2. Mössbauer characterization

In order to identify the iron species produced from our recipe, the Mössbauer spectra of sample M1 were registered at temperatures 263, 80, 30 and 13 K. The spectra are shown in figure 6 and their hyperfine parameters can be seen in table 4. The spectrum recorded at 13 K shows six lines with their inner sides slightly broadened and a central non-resolved signal. This spectrum was fitted to two sextuplets and two doublets with parameter distributions. The hyperfine parameters of both sextuplets can be attributed to Fe^{3+} ions located in tetrahedral (A) and octahedral (B) sites of γ-Fe_2O_3 [26]. The presence of Fe^{2+} ions was not detected. This result rules out the existence of Fe_3O_4. The hyperfine magnetic fields of both sites in the 8.8 nm γ-Fe_2O_3 NPs are decreased in comparison with the bulk values [26]. This effect could be assigned to the collective magnetic excitation phenomenon observed in very small particles below the blocking temperature [27].

The two doublets at 13 K can hardly be assigned to γ-Fe_2O_3 with sizes smaller than 8.8 nm. Indeed, they are expected to be blocked due its large anisotropy constant of about 2×10^4 erg cm^{-3} [28]. Recently, it had been found that Fe^{3+} surface ions can be complexed with oleic acid through carboxylate heads with monodentate and bidentate coordination [29, 30] and with alkylamine surfactants through $-NH_2$ groups [20]. As will be explained below, the FT-IR results allow us to discard the presence of oleic acid in

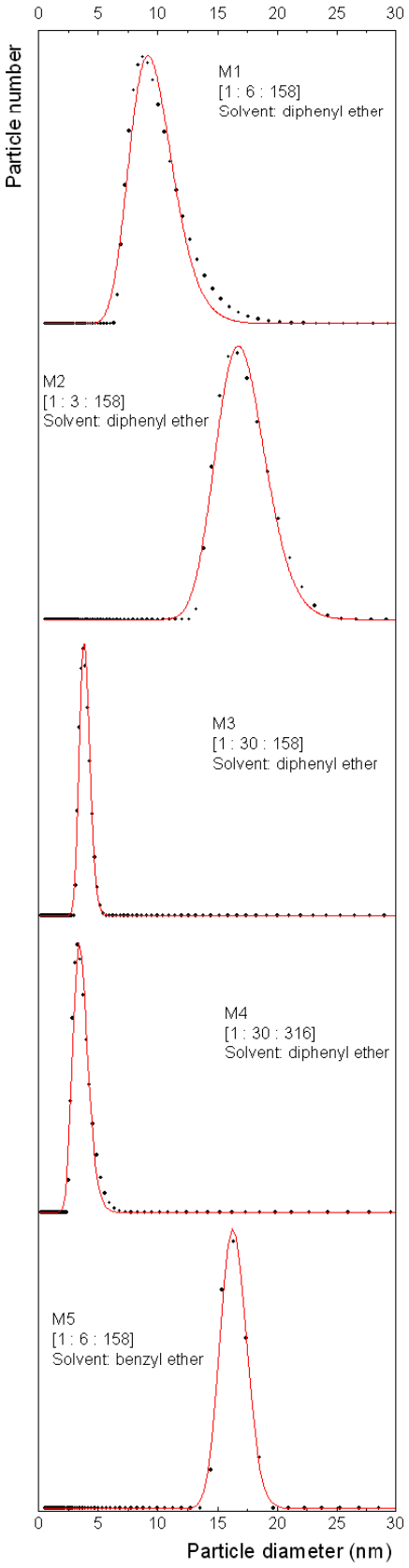

Figure 5. Size distributions of samples M1, M2, M3, M4 and M5 from DLS-QELS measurements from number averages. The molar ratio of iron salt:surfactant:solvent used in each synthesis is shown between brackets. Solid (red) lines were obtained fitting the results with a log-normal distribution.

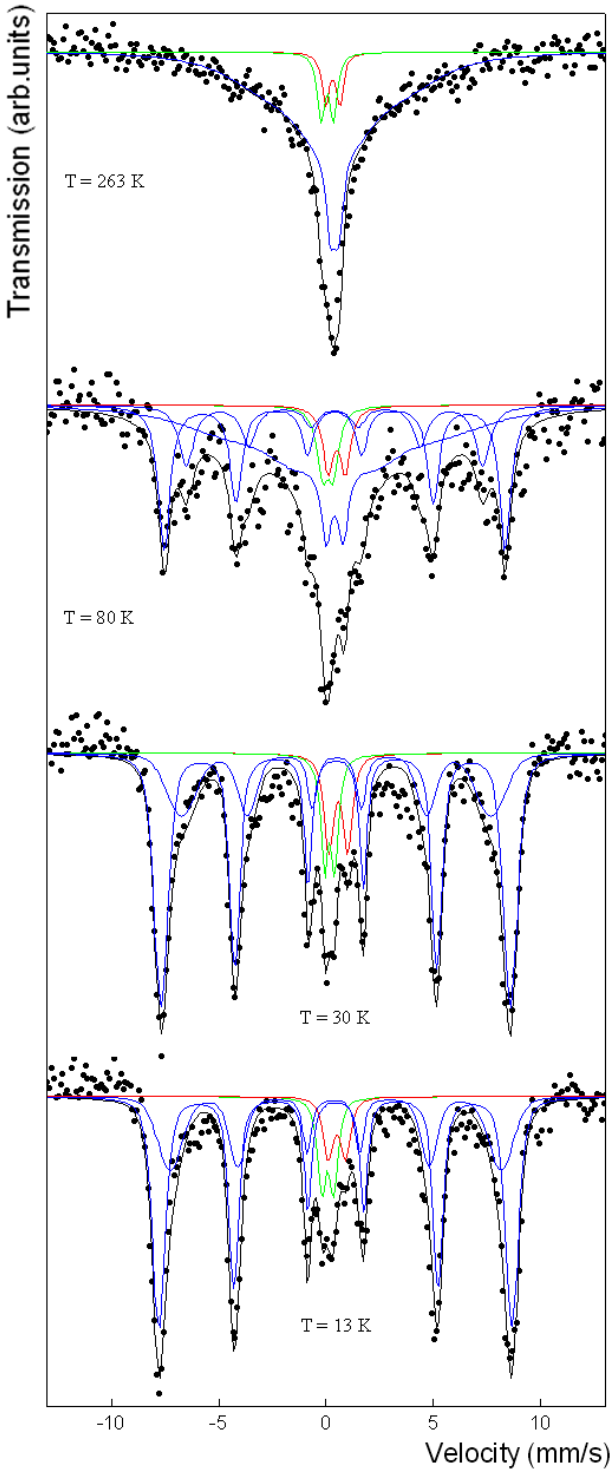

Figure 6. Mössbauer spectra of M1 NPs at different temperatures.

monodentate coordination with Fe^{3+} ions. It is important to remark that the isomer shift of one of the doublets is very small ($\delta = 0.08 \pm 0.06$ mm s^{-1}) in comparison with the typical values of high spin Fe^{3+} ions at low temperature (about 0.4–0.5 mm s^{-1}). This result would indicate an increase of the covalence of the iron bond in the presence of ligands (an increase of 4s electron density in the iron nucleus). The strong

Table 4. Hyperfine Mössbauer parameters of M1 sample at different temperatures. H, hyperfine magnetic field; δ, isomer shift (all the isomer shifts are referred to α-Fe at 298 K); 2ε, quadrupole shift; Δ, quadrupole splitting.

Species	Parameters	263 K	80 K	30 K	13 K
γ-Fe_2O_3 sites A	H (kG)	—	428 ± 8	447 ± 11	478[a]
	δ (mm s^{-1})	—	0.4[a]	0.49 ± 0.08	0.39 ± 0.05
	2ε (mm s^{-1})	—	0[a]	-0.1 ± 0.1	0.1 ± 0.1
	%	—	15 ± 4	27 ± 4	30 ± 3
γ-Fe_2O_3 sites B	H (kG)	—	492 ± 3	505 ± 1	510 ± 1
	δ (mm s^{-1})	—	0.4[a]	0.45 ± 0.02	0.44 ± 0.01
	2ε (mm s^{-1})	—	0[a]	0.00 ± 0.03	-0.02 ± 0.03
	%	—	29 ± 3	57 ± 3	56 ± 3
'Relaxing signal'	H (kG)	300[a]	450[a]	—	—
	δ (mm s^{-11})	0.39 ± 0.06	0.4[a]	—	—
	2ε (mm s^{-1})	0[a]	0[a]	—	—
	%	86 ± 5	44 ± 8	—	—
Superficial Fe^{3+} coordinated with oleylamine	Δ (mm s^{-1})	0.59 ± 0.06	0.5[a]	0.48 ± 0.08	0.56 ± 0.09
	δ (mm s^{-1})	0.06 ± 0.06	0.08[a]	0.16 ± 0.05	0.08 ± 0.06
	%	8[a]	6[a]	8 ± 2	8 ± 2
Superficial Fe^{3+} coordinated with oleic acid	Δ (mm s^{-1})	0.66[a]	0.8[a]	0.9 ± 0.1	0.8 ± 0.1
	δ (mm s^{-1})	0.31[a]	0.5[a]	0.57 ± 0.06	0.50 ± 0.09
	%	6[a]	6[a]	8 ± 2	6 ± 2

[a] Parameters held fixed in fitting.

Lewis basicity, characteristic of the amino groups, would allow assignment of the doublet with lower δ to superficial Fe^{3+} ions coordinated with oleylamine. On the other hand, the other doublet could be assigned to superficial Fe^{3+} ions coordinated with oleic acid in a bidentate way. When the temperature is increased from 13 to 30 K, no significant changes occur in hyperfine parameters and percentages of signals. Therefore, we can conclude that at 30 K the NPs are magnetically blocked in a complete way. This confirms that the central doublets do not belong to superparamagnetic γ-Fe_2O_3 NPs. Instead, at 80 K, magnetic relaxation phenomena are taking place, making it necessary to include a relaxing signal in the fitting procedure. At this temperature, the areas of the blocked and relaxing signals assigned to γ-Fe_2O_3 are equal ($44 \pm 7\%$ and $44 \pm 8\%$ respectively). The temperature at which the superparamagnetic relaxation time is equal to the timescale of the experimental technique is called the blocking temperature, T_B. Therefore, we can estimate that the Mössbauer T_B of the M1 sample is about 80 K. Finally, at 263 K, almost the entire population of the NPs is in a superparamagnetic regime and the sextuplets have collapsed to a central signal.

In single-domain particles—with superparamagnetic relaxation—the magnetization direction fluctuates spontaneously and the relaxation time (τ) exhibits an exponential dependence on temperature characterized by a Néel–Arrhenius law [31]:

$$\tau = \tau_0 \exp\left(\frac{E_a}{k_B T}\right) \tag{1}$$

where T is the temperature, k_B is Boltzmann's constant and E_a is the anisotropy energy barrier. For negligible interparticle interactions, τ_0 in maghemite nanoparticles is of the order of 10^{-10} s [28]. In the absence of an external magnetic field, the energy barrier can be assumed to be proportional to the particle volume V, and if NPs have a dominating uniaxial anisotropy it is given by

$$E_a = K_{eff} V \sin^2\theta \tag{2}$$

where K_{eff} is an effective magnetic anisotropy constant and θ is the angle between the magnetic moment of the particle and its easy magnetization axis. When T_B is reached, the relaxation time can be considered equal to the characteristic measurement time of the used technique. If Mössbauer spectroscopy is used, this time is equal to the nuclear Larmor precession time, $\tau_L \approx 2.5$ ns. Therefore, a value of $K_{eff} = 1 \times 10^5$ erg cm^{-3} is obtained. Assuming a cubic anisotropy, considering that the easy axis is the [111] direction and the second order magnetocrystalline anisotropy constant, K_2, is negligible, the ratio between K_{eff} and the first order magnetocrystalline anisotropy constant, K_1, is $K_{eff} = -K_1/12$. Therefore, a value of $K_1 = (-1.2 \times 10^6$ erg $cm^{-3})$ is obtained. However, in maghemite, the first order magnetocrystalline anisotropy constant, K_1, is approximately equal to $(-2.5 \times 10^5$ erg $cm^{-3})$ [28]. Other contributions could enlarge the effective magnetic anisotropy constant, such as shape and surface anisotropy. However, taking into account that M1 NPs are nearly spherical, the shape anisotropy contribution is zero [32]. On the other hand, the ratio between K_{eff} and the bulk anisotropy energy per unit volume (K_V), and the surface density of anisotropy energy (K_S) for spherical particles of diameter d, was presented by Bødker *et al* [33]:

$$K_{eff} = K_V + \frac{6}{d} K_s\,. \tag{3}$$

From symmetry arguments, and assuming that surface anisotropy is normal to the particle surface, these authors have

demonstrated that a perfect spherical particle should have a zero net contribution from surface anisotropy. This model was verified by Komorida *et al* [28], who found that the surface contribution is about two orders of magnitude lower than K_V in maghemite NPs of 5 nm. Therefore, our result of about one order of magnitude larger than the magnetocrystalline anisotropy constant of bulk maghemite can be attributed to the existence of dipolar magnetic interactions, which can decrease dramatically the τ_0 values [28, 34]. The existence of these interactions will be confirmed by magnetic measurements, as will be described below.

3.3. Analysis of FT-IR spectra

To get insight about the possibility that Fe^{3+} ions on the NP surface are coordinated with oleic acid and oleylamine molecules, we have obtained the FT-IR spectra of pure oleic acid and oleylamine and M3 NPs after purification treatment. We chose this NP batch since its particles are the smallest ones obtained in the present work. Therefore, they have the largest surface/volume ratio and they could produce more intense signals of the coordinated surface molecules. Figure 7 presents the FT-IR spectra of oleic acid, oleylamine and M3 NPs. Both pure oleic acid and oleylamine, show characteristic modes of oleyl groups: peaks at 2851–2853 and 2922–2925 cm^{-1} are due to the symmetric and asymmetric CH_2 stretching modes respectively, and peaks at 3003–3006 cm^{-1} are assigned to the ν(C–H) mode of the C–H bond adjacent to the C=C bond [35]. A weak peak at 1650–1657 cm^{-1} is due to the ν (C=C) stretching mode [35]. All these bands were detected in the FT-IR spectrum of M3.

Furthermore, the spectrum of the pure oleic acid shows characteristic modes of the carboxylic acid group: the ν (C=O) mode is observed at 1707 cm^{-1} and the weak mode at 2674 cm^{-1} is attributed to the ν(O–H) stretch of the dimerized acid [35, 36]. The broad shoulder in the region between 3100 and 3500 cm^{-1} could be assigned to dimers of oleic acid in a bilayer structure [29].

On the other hand, oleylamine displays typical modes of amine groups: the peak at 1576 cm^{-1} is due to the NH_2 scissoring mode and the peak at about 3300 cm^{-1} is assigned to the ν(N–H) stretching mode [37].

The FT-IR spectrum of M3 NPs did not show the typical band of carbonyl group of oleic acid at 1707 cm^{-1}. Therefore, the possibility of monodentate coordination of oleic acid with superficial Fe^{3+} ions can be discarded, since this coordination implies the presence of carbonyl groups [29]. On the other hand, the characteristic IR bands for metal carboxylates are in the range of 1650–1510 cm^{-1} for the asymmetrical vibrations and 1400–1280 cm^{-1} for the symmetrical vibrations [38]. Clearly, M3 shows two bands at 1562 and 1525 cm^{-1}. Both of them are absent from the IR oleic acid spectrum, and the second one is absent in the oleylamine spectrum. The situation is less obvious with the 1425 cm^{-1} band, since pure oleic acid presents peaks between 1460 and 1416 cm^{-1}. Notwithstanding, the present results confirm the existence of superficial iron carboxylate species. Furthermore, the separation of metal carboxylate bands (Δ),

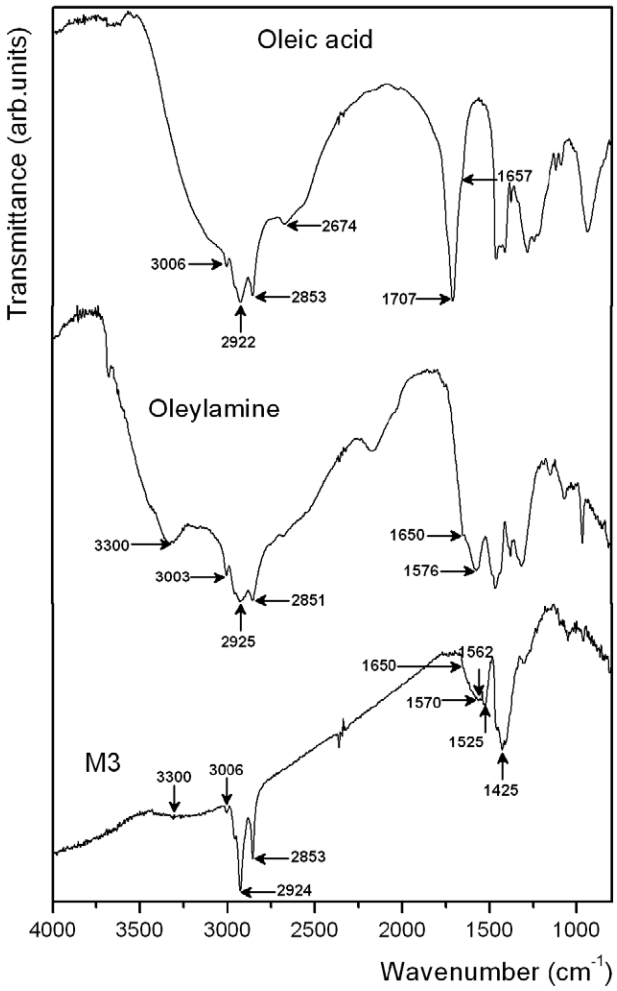

Figure 7. FT-IR spectra of pure oleic acid, pure oleylamine and M3 NPs.

in the 1300–1700 cm^{-1} region, can be used to deduce the carboxylate coordination mode [38]. For $\Delta > 200$ cm^{-1} a monodentate ligand is expected, for $\Delta < 110$ cm^{-1} it is a bidentate ligand and for 140 $cm^{-1} < \Delta < 200$ cm^{-1} a bridging ligand exists. For M3, the differences between the characteristic carboxylate bands shown in figure 7 are 37, 100 and 137 cm^{-1}, which reveal a bidentate coordination. These species would produce the Mössbauer doublet with the higher δ as explained before.

There is less evidence of the presence of oleylamine coordinated with superficial iron atoms of the NPs, since the typical peak at 1576 cm^{-1} (due to the NH_2 scissoring mode) just appears as a small shoulder of the 1562 cm^{-1} peak. Notwithstanding, in the region of 3300 cm^{-1} (characteristic of ν(N–H) stretching mode) a broad poorly defined signal appears. However, this result is not conclusive because, in the same region, the signal corresponding to dimers of oleic acid can be detected. Maybe the quantity of oleylamine molecules bonded to Fe^{3+} superficial ions is lower than that corresponding to oleic acid. However, the presence of both ligands bonded to Fe^{3+} ions is compatible with the present FT-IR spectrum. This result is coherent with the Mössbauer assignments.

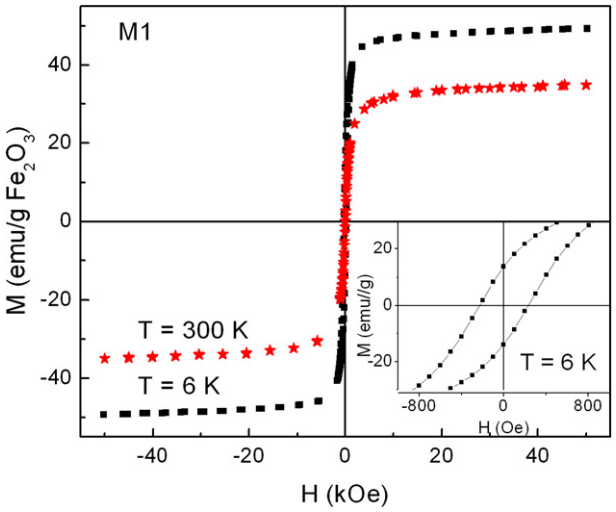

Figure 8. *M* versus *H* loops at 300 and 6 K for M1 NPs. The inset shows the remanence and coercivity at 6 K.

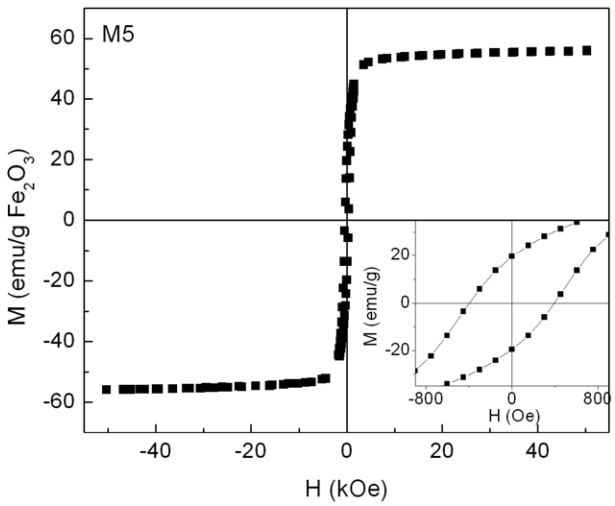

Figure 9. *M* versus *H* loop at 6 K for M5 NPs. The inset shows the remanence and coercivity at 6 K.

3.4. Magnetic properties

The magnetic characterization was performed on M1 and M5 samples, which represent the sets of NPs with smaller and larger average sizes, respectively. *M* versus *H* loops of M1 NPs are shown in figure 8. The saturation magnetization (M_s) at 6 K is 49 emu per gram of γ-Fe_2O_3. The coercive field (H_c) at this temperature is $H_c = 230$ Oe, while the remanence (M_r) is about 14 emu per gram of γ-Fe_2O_3. At 298 K, the relatively low $H_c = 15$ Oe would indicate that most of the NPs are in a superparamagnetic regime. This result is coincident with that obtained by Mössbauer spectroscopy at 263 K. M_s is about 34% lower than the bulk phase (about 74 emu per gram of γ-Fe_2O_3 [39]). This effect has usually been reported, the first studies on the M_s decreases in γ-Fe_2O_3 being reported by Coey [40]. This author showed that the reduction is due to the existence of non-collinear spins at the surface of the particles. Furthermore, Morales *et al* [41] have found that differences in the order–disorder characteristics of the samples also have a strong influence on the M_s values of small maghemite particles.

In the case of sample M5, M_s at 6 K is about 56 emu per gram of γ-Fe_2O_3 (figure 9). At this same temperature, $H_c = 400$ Oe and M_r is about 20 emu per gram of γ-Fe_2O_3. These higher magnetic parameter values are in accordance with the larger particle sizes.

At $T = 6$ K, the remanence-to-saturation ratios $R = M_r/M_s$ for both M1 ($R = 0.28$) and M5 ($R = 0.38$) samples are lower than the expected $R = 0.5$ value for non-interacting, randomly oriented particles with uniaxial symmetry. Therefore, this result, in agreement with the Mössbauer spectroscopy ones, reveals the existence of interparticle interactions [42].

Assuming that the particles are non-interacting and have uniaxial magnetocrystalline anisotropy, the coercivity field is related to the effective anisotropy constant through the relation $H_c = 2K_{eff}/M_s$ [43]. From this, we obtain $K_{eff} = 2.7 \times 10^4$ erg cm^{-3} for M1, which gives a first order magnetocrystalline anisotropy constant, $K_1 = -3.2 \times 10^5$ erg cm^{-3}. This result agrees quite well with K_1 of bulk maghemite ($K_1 = -2.5 \times 10^5$ erg cm^{-3}). However, the K_{eff} values obtained from Mössbauer spectroscopy and magnetic measurements differ by about one order of magnitude. This can be interpreted considering that the Mössbauer data are dynamic, in the absence of an external magnetic field. Instead, the value obtained from magnetic measurements implies the existence of an external magnetic field. Therefore, the former should be largely affected by the presence of dipolar interactions, whereas the latter is essentially determined by the external field. It is interesting to analyse that, due to the covering of the NPs with oleic acid (considering that oleylamine is a minority component, as deduced from the FT-IR results), the minimum distance between the surface of two neighbour NPs would be about 3.0 nm, taking into account that the chain length of oleic acid is about 1.5 nm [44]. This minimum distance could be obtained if an auto-assembly in a structure such as a lipidic bilayer is produced between the tails of the oleic acid molecules coordinated with two neighbour NPs (as suggested from the FT-IR results). This situation is schematically represented in figure 10. From this rough model, it can be deduced that a separation of about

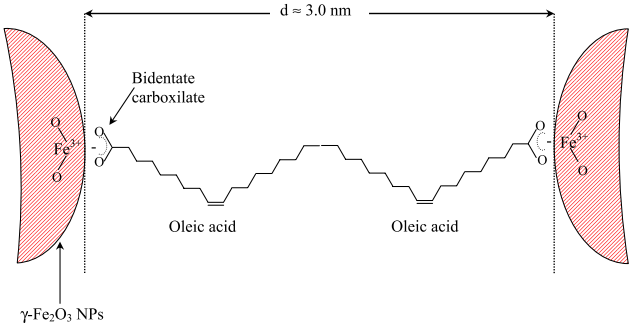

Figure 10. Schematic representation of the NPs, covered by oleic acid in an arrangement at minimum distance between them.

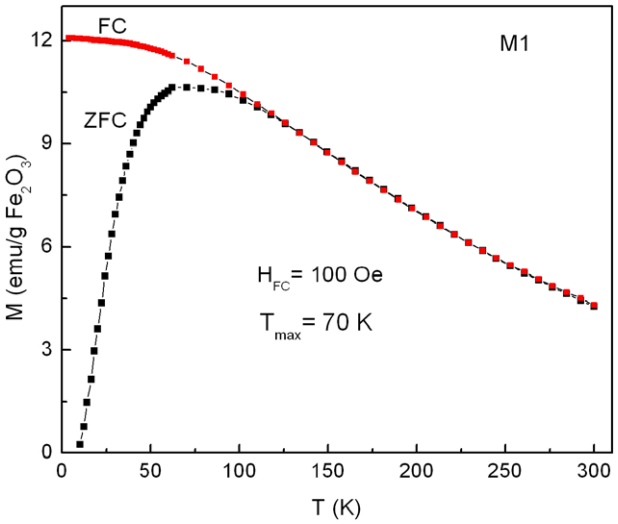

Figure 11. ZFC–FC magnetization curves for M1 NPs.

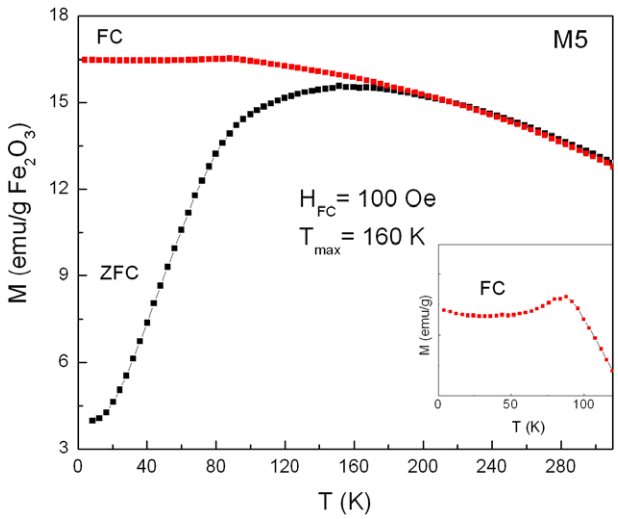

Figure 12. ZFC–FC magnetization curves for M5 NPs.

3.0 nm, in γ-Fe_2O_3 NPs of 8.8 nm average diameter, is not enough to inhibit the magnetic interparticle interactions.

ZFC and FC magnetization curves of M1 and M5 samples are shown in figures 11 and 12 respectively. The behaviour is typical of an arrangement of superparamagnetic nanoparticles, whose magnetic moments block progressively when the temperature decreases, according to the distribution of their blocking temperatures. The ZFC magnetization of M1 shows a maximum at $T_{max} = 70$ K, which is associated with the average blocking temperature $\langle T_B \rangle$ by the following equation:

$$T_{max} = \beta \langle T_B \rangle \tag{4}$$

where β is a proportionality constant, depending on the type of size distribution. For a log-normal distribution, the value of β is typically in the range 1.5–2.5 [45, 46]. Considering this range of β values, $\langle T_B \rangle$ is between 28 and 47 K. For M5, the maximum of ZFC magnetization at $T_{max} = 160$ K (figure 12) implies that $\langle T_B \rangle$ is between 64 and 107 K. These higher $\langle T_B \rangle$ values and the broader ZFC curve observed for M5 reflects the higher anisotropy energy barrier connected with the larger average particle size (16.3 nm) as well as with interactions.

The FC and ZFC curves split below a temperature called the irreversibility temperature (T_{irr}), which is associated with the blocking of the largest particles. We take T_{irr} as the temperature where the difference between FC and ZFC curves, normalized to its maximum value at $T = 4$ K, becomes smaller than 3% [45, 47]. For the M1 sample, $T_{irr} = 86$ K. The difference between T_{irr} and T_{max} provides a measure of the width of the blocking temperature distribution and then of the particle size distribution, assuming the same anisotropy constant and absence of interparticle interactions. In the present sample, $T_{irr} - T_{max} = 15$ K, which would confirm the existence of a narrow size distribution. Even though DLS-QELS results indicate that the M5 sample has a narrower size distribution, in this case $T_{irr} - T_{max} = 40$ K, probably due to stronger interparticle interaction effects as described below.

Finally, we observe that below about 50 K the FC curve corresponding to M1 is flattened. This would indicate that interparticle interactions are present in this sample. The FC curve of M5 presents a similar but more pronounced feature. In addition, a different behaviour can be appreciated for M5, where its FC magnetization shows a declination at low temperatures, showing a maximum at about 90 K (see inset in figure 12). This behaviour has been previously reported to occur in iron oxide NPs [48, 49] and is usually observed in spin glass systems. In our case, it would reflect a collective freezing process of strongly interacting particle moments [48, 49]. The absence of this feature in the FC curve of M1 taken under the same field $H_{FC} = 100$ Oe reveals its weaker local anisotropy due to the lower strength of their interactions.

4. Conclusions

In the present work, a new approach to thermal decomposition of organic iron precursors, in order to get a more simple and economical method to produce well crystallized γ-Fe_2O_3 NPs, is reported. This new method represents a saving of about 86% of the total reagent cost in comparison with the original recipes. Furthermore, the handling of the reagents is easier since an inert atmosphere is unnecessary. It was shown that, changing operative variables, it is possible to modify the average particle diameters with very narrow or monodispersed distribution sizes. These results are very important in order to produce future technological applications since it is indispensable to consider the existence of scale change demand. The obtained γ-Fe_2O_3 NPs are superparamagnetic at room temperature and they are covered by oleic acid (coordinated in a bidentate way) and, in a lower quantity, by oleylamine. The distance between two neighbour NPs generated by this covering is insufficient to inhibit interparticle magnetic interactions when the average diameter is 8.8 nm. This result is important when it is necessary to determine magnetic fundamental properties such as anisotropy constants, blocking temperatures, etc. Finally,

the magnetization saturation is decreased by about 34% for the sample with the smallest average size with respect to the bulk phase.

Acknowledgment

The authors acknowledge the financial support of ANPCyT (PICT No 00549), which allowed the development of this work.

References

[1] Jain T K, Morales M A, Sahoo S K, Leslie-Pelecky D L and Labhasetwar V 2005 *Mol. Pharm.* **2** 194–205
[2] Chourpa I, Douziech-Eyrolles L, Ngaboni-Okassa L, Fouquenet J F, Cohen-Jonathan S, Souce M, Marchais H and Dubois P 2005 *Analyst* **130** 1395–03
[3] Lee K-B, Park S and Mirkin C A 2004 *Angew. Chem. Int. Edn* **43** 3048–50
[4] Mura C V, Becker M I, Orellana A and Wolff D J 2002 *J. Immunol. Methods* **260** 263–71
[5] Kim D K, Zhang Y, Kehr J, Klason T, Bjelke B and Muhammed M 2001 *J. Magn. Magn. Mater.* **255** 256–61
[6] Modo M M J and Bulté J W M 2007 *Molecular and Cellular MR Imaging* ed M M J Modo and J W M Bulté (Boca Raton, FL: CRC Press)
[7] Burtea C, Laurent S, Roch A, Vander Elst L and Muller R N 2005 *J. Inorg. Biochem.* **99** 1135–44
[8] Fortin J P, Wilhelm C, Servais J, Menager C, Bacri J C and Gazeau F 2007 *J. Am. Chem. Soc.* **129** 2628–35
[9] Sun S, Murray C, Weller D, Folks L and Moser A 2000 *Science* **287** 1989–92
[10] Sun S and Zeng H 2002 *J. Am. Chem. Soc.* **124** 8204–5
[11] Peikov V T, Jeon K S and Lane A M 1999 *J. Magn. Magn. Mater.* **193** 307–10
[12] McMichael R D, Shull R D, Swartzendruber L J, Bennet L H and Watson R E 1992 *J. Magn. Magn. Mater.* **111** 29–33
[13] Guin D, Baruwati B and Manorama S V 2007 *Org. Lett.* **9** 1491–21
[14] Gupta A K and Wells S 2004 *IEEE Trans. Nanobiosci.* **3** 66–73
[15] Teja A S and Koh P-Y 2009 *Prog. Cryst. Growth Charact. Mater.* **55** 22–45
[16] Veintemillas-Vendaguer S *et al* 2004 *J. Phys. D: Appl. Phys.* **37** 2054–9
[17] Li Z, Chen H, Bao H and Gao M 2004 *Chem. Mater.* **16** 1391–3
[18] Rockenberger J, Scher E C and Alivisatos A P 1999 *J. Am. Chem. Soc.* **121** 11595–6
[19] Hyeon T, Lee S S, Park J, Chung Y and Na H B 2001 *J. Am. Chem. Soc.* **123** 12798–01
[20] Sun S, Zeng H, Robinson D B, Raoux S, Rice P M, Wang S X and Li G 2004 *J. Am. Chem. Soc.* **126** 273–9
[21] Provencher S W 1982 *Comput. Phys. Commun.* **27** 213–27
[22] Lagarec V and Rancourt D G 1998 *Mossbauer Spectral Analysis Software* Dep. of Phys. University of Otawa, Version 1.0
[23] Sandell E B 1959 *Colorimetric Determination of Traces of Metals* 3rd edn (New York: Interscience Publishers)
[24] Granqvist C G and Buhrman R A 1976 *J. Appl. Phys.* **47** 2200–19
[25] Zhu Y, Jiang F Y, Chen K, Kang F and Tang Z K 2011 *J. Alloys Compounds* **509** 8549–53
[26] Murad E 1998 *Hyperfine Interact.* **117** 39–70
[27] Mørup S and Topsøe H 1976 *Appl. Phys.* **11** 63–6
[28] Komorida Y, Mito M, Deguchi H, Takagi S, Millán A, Silva N J O and Palacio F 2009 *Appl. Phys. Lett.* **94** 202503
[29] Bronstein L M, Huang X, Retrum J, Schmucker A, Pink M, Stein B D and Dragnea B 2007 *Chem. Mater.* **19** 3624–32
[30] Lin M M and Kim D K 2012 *J. Nanopart. Res.* **14** 688–705
[31] Néel L 1949 *Ann. Geophys.* **5** 99–136
[32] Mørup S and Hansen M F 2007 *Handbook of Magnetism and Advanced Magnetic Materials Vol 4: Novel Materials* ed H Kronmüller and S Parkin (New York: Wiley) p 2179
[33] Bødker F, Mørup S and Linderoth S 1994 *Phys. Rev. Lett.* **72** 282–5
[34] Dormann J L, D'Orazio F, Lucari F, Tronc E, Prené P, Jolivet J P, Fiorani D, Cherkaoui R and Nogués M 1996 *Phys. Rev.* B **53** 14291–7
[35] Lee D H, Condrate R A Sr and Lacourse W C 2000 *J. Mater. Sci.* **35** 4961–70
[36] Lee D H and Condrate R A Sr 1999 *J. Mater. Sci.* **34** 139–46
[37] Erley W and Hemminger J C 1994 *Surf. Sci.* **316** L1025–30
[38] Lu Y and Miller J D 2002 *J. Colloid Interface Sci.* **256** 41–52
[39] Feltin N and Pileni M P 1997 *Langmuir* **13** 3927–33
[40] Coey J M D 1971 *Phys. Rev. Lett.* **27** 1140–2
[41] Morales M P, Andres-Vergés M, Veintemillas-Verdaguer S, Montero M I and Serna C J 1999 *J. Magn. Magn. Mater.* **203** 146–8
[42] Hadjipanayis G, Sellmyer D J and Brandt B 1981 *Phys. Rev.* B **23** 3349–54
[43] Goya G F, Berquo T S, Fonseca F C and Morales M P 2003 *J. Appl. Phys.* **94** 3520–8
[44] Yang K, Peng H, Wen Y and Li N 2010 *Appl. Surf. Sci.* **256** 3093–7
[45] Peddis D, Mansilla M V, Mørup S, Cannas C, Musinu A, Piccaluga G, D'Orazio F, Lucari F and Fiorani D 2008 *J. Phys. Chem.* B **112** 8507–13
[46] Gittleman J L, Abels B and Bozowski S 1974 *Phys. Rev.* B **9** 3891–7
[47] Del Bianco L, Fiorani D, Testa A M, Bonetti E, Savini L and Signoretti S 2002 *Phys. Rev.* B **66** 174418
[48] Zysler R D, Fiorani D and Testa A M 2001 *J. Magn. Magn. Mater.* **224** 5–11
[49] Leite E S, Coaquira J A H, Viali W R, Sartoratto P P C, de Almeida R L, Morais P C and Malik S K 2010 *J. Phys.: Conf. Ser.* **200** 072060